

Self-consistent treatment of dynamical correlation functions using a spectral representation technique

M. Letz^a and F. Marsiglio^b

^a Institut für Physik, Johannes-Gutenberg Universität, 55099 Mainz, Germany

^b Department of Physics, University of Alberta, Edmonton, Alberta, Canada T6G 2J1
(April 9, 2017)

A system of equations resulting from an approximation of the equation of motion of Green functions for correlated electron systems is usually solved using Matsubara technique. In this work we propose an alternative method which works entirely along the real frequency axis. Using the example of the attractive Hubbard model studied in the T-matrix approximation both self-consistently and non-self-consistently we demonstrate how powerful such a treatment is especially when dynamic quantities are calculated.

74.20 Mn 74.25.-q 74.20-z

I. INTRODUCTION

When investigating systems in thermodynamic equilibrium with time independent Hamiltonians it was a great success to solve and discuss correlation functions in the transformed frequency space. These functions are analytic functions in the complex plane except for a branch cut along the real axis. This knowledge was first used for the T=0 Green function technique e.g. [1,2]. However, especially for finite temperatures, the theory of complex differentiable functions had led to the development of a very powerful method, the Matsubara technique [3].

For the derivation of the equations of motion an imaginary axis formulation using Matsubara frequencies was used very early. The numerical solution of such equations however was first achieved along the real axis. An example for this is the solution of the Eliashberg equations by Schrieffer et al. [4,5].

Later it was discovered that a numerical solution was far more efficient when an imaginary axis technique is used. In this way static quantities like e.g. expectation values for occupation numbers (n) or double occupancy ($\langle n_{\uparrow}n_{\downarrow} \rangle$) and their temperature dependence and some thermodynamic quantities can be calculated successfully. An example is the calculation of the the superconducting critical temperature [6,7] and the temperature dependence of the critical magnetic field and specific heat from the Eliashberg equations [8].

A major shortcoming of such an imaginary axis treatment is that dynamical quantities like, for example, the electron density of states (along the real frequency axis) are difficult to obtain. Usually Pade approximants [9] or maximum entropy [10] techniques are used to obtain dynamical quantities. The fact that we need these complicated methods shows how difficult it is to calculate the values of a function at n^R points along the real axis when n^I points along the imaginary axis are known. The simplest way to illustrate this is the following: The further away the n^I points are from the n^R points the more the system of equations which has to be solved in order to obtain dynamical quantities tends to be singular

and therefore tiny inaccuracies of the functions on the n^I points, the Matsubara frequencies, can lead to much bigger inaccuracies along the real axis, at points n^R .

In this paper we go in some sense back to the old real axis technique and propose a treatment in which all quantities are directly calculated along the real axis. Since we do not calculate the functions at the Matsubara frequencies we do not need a mapping onto the real axis. As an example we use the T-matrix calculation using the ladder diagrams in the particle-particle channel for the attractive Hubbard model. This approximation is valid in the low density regime and is of particular interest since it might be able to model some aspects of the short coherence length pairs observed in the high- T_c superconductors [11–13].

II. SPECTRAL REPRESENTATIONS

In order to motivate our method we give here a short overview of how different treatments of Green functions can be connected by using a spectral representation and by using the whole frequency plane.

A one particle correlation function of operators C and B which are either both Bosonic or Fermionic operators can be written as a function of temporal and spatial coordinates:

$$G^k(x_i, t, x_j, t') = -i \langle T_{F/B} C^\dagger(x_i, t) B(x_j, t') \rangle \quad (1)$$

where $T_{F/B}$ is the time ordering operator for Fermions or Bosons and

$$\langle \dots \rangle = Z^{-1} Tr(e^{-\beta \bar{H}} \dots) \quad (2)$$

is the thermal expectation value. Z is the partition function in the grand canonical ensemble and $\bar{H} = H - \mu N$ is the Hamiltonian in this ensemble. If we restrict ourselves to systems in thermal equilibrium with periodic boundary conditions and time independent Hamiltonians we can apply a Fourier transform [14]:

$$G^k(\mathbf{k}, \omega) = \int_{-\infty}^{\infty} d(t-t') \frac{1}{N} \int d(\mathbf{x}_i - \mathbf{x}_j) G^{rk}(t-t', x_i - x_j) e^{i\omega(t-t')} e^{i\mathbf{k}(\mathbf{x}_i - \mathbf{x}_j)} \quad (3)$$

The definition (1) and equation (3) are valid at all temperatures.

The function $G^k(\mathbf{k}, \omega)$ is related to a function which is analytic in the whole complex ω -plane with the exception of a branch cut along the real axis. Therefore there exists a spectral representation and $G^k(\mathbf{k}, \omega)$ can be rewritten as a function of a spectral function $J(\mathbf{k}, \omega)$ which is a real function defined along the real ω axis. The Green function $G^k(\mathbf{k}, \omega)$ is connected to its spectral representation in the following way:

$$G^k(\mathbf{k}, \omega) = \lim_{\delta \rightarrow 0^+} \frac{1}{2\pi} \int_{-\infty}^{\infty} d\bar{\omega} \left(\frac{J(\mathbf{k}, \bar{\omega}) e^{\beta\bar{\omega}}}{\omega - \bar{\omega} + i\delta} - \frac{\mp J(\mathbf{k}, \bar{\omega})}{\omega - \bar{\omega} - i\delta} \right) \quad (4)$$

Here and in the following the upper sign corresponds to Fermions whereas the lower sign describes Bosons. For practical use we want to define a slightly different function $A(\mathbf{k}, \omega)$:

$$A(\mathbf{k}, \omega) = \frac{1}{2} J(\mathbf{k}, \omega) (e^{\beta\omega} \pm 1) \quad (5)$$

Therefore equation (4) can be rewritten:

$$G^k(\mathbf{k}, \omega) = \lim_{\delta \rightarrow 0^+} \frac{1}{\pi} \int_{-\infty}^{\infty} d\bar{\omega} \left(\frac{A(\mathbf{k}, \bar{\omega}) \frac{e^{\beta\bar{\omega}}}{e^{\beta\bar{\omega}} \pm 1}}{\omega - \bar{\omega} + i\delta} \pm \frac{A(\mathbf{k}, \bar{\omega}) \frac{1}{e^{\beta\bar{\omega}} \pm 1}}{\omega - \bar{\omega} - i\delta} \right) \quad (6)$$

For a non-interacting system and C, B e.g. Fermionic operators $c_{\mathbf{k}}$ the function $\sum_{\mathbf{k}} A(\mathbf{k}, \omega)$ is identical to the density of states. For an interacting system $\sum_{\mathbf{k}} A(\mathbf{k}, \omega)$ will still be a density of states but $A(\mathbf{k}, \omega)$ becomes dependent on the thermodynamic variables T, μ .

$$A(\mathbf{k}, \omega) \longrightarrow A^{T, \mu}(\mathbf{k}, \omega) \quad (7)$$

The usual $T = 0$ Green functions for which the zero temperature diagram technique [15] is valid can be rewritten as a function of $A^{T, \mu}(\mathbf{k}, \omega)$:

$$G^k(\mathbf{k}, \omega) = \lim_{\beta \rightarrow \infty} \lim_{\delta \rightarrow 0^+} \frac{1}{\pi} \int_{-\infty}^{\infty} d\bar{\omega} \left(\frac{A^{T, \mu}(\mathbf{k}, \bar{\omega}) \frac{e^{\beta\bar{\omega}}}{e^{\beta\bar{\omega}} \pm 1}}{\omega - \bar{\omega} + i\delta} \pm \frac{A^{T, \mu}(\mathbf{k}, \bar{\omega}) \frac{1}{e^{\beta\bar{\omega}} \pm 1}}{\omega - \bar{\omega} - i\delta} \right) \quad (8)$$

$$G^R(\mathbf{k}, \omega) = \lim_{\beta \rightarrow \infty} \lim_{\delta \rightarrow 0^+} \frac{1}{\pi} \int_{-\infty}^{\infty} d\bar{\omega} \frac{A^{T, \mu}(\mathbf{k}, \bar{\omega})}{\omega - \bar{\omega} + i\delta} \quad (9)$$

$$G^A(\mathbf{k}, \omega) = \lim_{\beta \rightarrow \infty} \lim_{\delta \rightarrow 0^+} \frac{1}{\pi} \int_{-\infty}^{\infty} d\bar{\omega} \frac{A^{T, \mu}(\mathbf{k}, \bar{\omega})}{\omega - \bar{\omega} - i\delta} \quad (10)$$

where R, A denotes retarded and advanced Green functions. $G^R(\mathbf{k}, \omega)$ and $G^A(\mathbf{k}, \omega)$ are both branches of one function $G(\mathbf{k}, z)$ defined on the whole complex plane with the exception of the branch cut along the real axis where the poles of $A^{T, \mu}(\mathbf{k}, \bar{\omega})$ are located:

$$G(\mathbf{k}, z) = \frac{1}{\pi} \int_{-\infty}^{\infty} d\bar{\omega} \frac{A^{T, \mu}(\mathbf{k}, \bar{\omega})}{z - \bar{\omega}} \quad (11)$$

Also the thermal Green functions defined entirely along the imaginary frequency axis can be written as a function of $A^{T, \mu}(\mathbf{k}, \bar{\omega})$

$$G^t(\mathbf{k}, i\omega_n) = \frac{1}{\pi} \int_{-\infty}^{\infty} d\bar{\omega} \frac{A^{T, \mu}(\mathbf{k}, \bar{\omega})}{i\omega_n - \bar{\omega}} \quad (12)$$

where $i\omega_n = \frac{(2n+1)\pi i}{\beta}, \frac{2n\pi i}{\beta}$ are the Matsubara frequencies for Fermions and Bosons respectively. The fact that the functions are only defined at certain periodic points means that the Fourier series of eq. (12)

$$G^t(\mathbf{k}, i\tau) = \frac{1}{\beta} \sum_{n=-\infty}^{\infty} e^{-i\omega_n \tau} G^t(\mathbf{k}, i\omega_n) \quad (13)$$

is periodic in imaginary time

$$G^t(\mathbf{k}, i\tau + i\beta) = \mp G^t(\mathbf{k}, i\tau) \quad (14)$$

This means that the full knowledge of the function $G(\mathbf{k}, z)$ is either obtained by knowing (a) $G(\mathbf{k}, i\omega_n)$ on the infinite but discrete points $i\omega_n$ along the imaginary axis or by knowing (b) $A^{T, \mu}(\mathbf{k}, \omega)$ on a continuum along the real axis. The details of the usual Green function technique are outlined in many textbooks e.g. [16,15]. Here we only want to highlight the connection of both methods with the function $A^{T, \mu}(\mathbf{k}, \omega)$. The usual Matsubara technique determines the functions along the points $i\omega_n$ whereas we will discuss a method in this paper which calculates an approximation of $A^{T, \mu}(\mathbf{k}, \omega)$.

III. NUMERICAL TECHNIQUE

The solution of the equations in a certain approximation for a correlated quantum system will generally be found numerically. In order to achieve self-consistency it is preferable to perform discrete sums over Matsubara frequencies than to calculate a function like $A^{T, \mu}(\mathbf{k}, \omega)$. But to obtain dynamical quantities along the real axis, a difficult and somewhat uncontrolled analytic continuation will have to be performed. Therefore there have been attempts to solve such systems along the real axis (see for example [17] for the Eliashberg equations and [18,19] for the self-consistent T-matrix equations). In these works some numerical integration was required along the real axis.

However in this section we argue that it is possible to replace $A^{T, \mu}(\mathbf{k}, \omega)$ by a series of (typically a few hundred)

δ functions along the real axis. With this approximation all frequency integrations will turn into summations over a finite number of δ functions and can therefore be done analytically. We use

$$A^{T,\mu}(\mathbf{k}, \omega) \approx \pi \sum_{l=1}^{N_{max}} a_l^{\mathbf{k}} \delta(\omega - b_l) \quad (15)$$

where the amplitudes are $a_l^{\mathbf{k}}$ (which also depend on the thermodynamic variables) and the poles are located at the positions b_l . The Green function $G(\mathbf{k}, \omega)$ can now be expressed in this approximation as a sum of poles:

$$\begin{aligned} G(\mathbf{k}, i\omega_n) &\approx \frac{1}{\pi} \int_{-\infty}^{\infty} d\bar{\omega} \frac{\pi \sum_{l=1}^{N_{max}} a_l^{\mathbf{k}} \delta(\bar{\omega} - b_l)}{i\omega_n - \bar{\omega}} \\ &= \sum_{l=1}^{N_{max}} \frac{a_l^{\mathbf{k}}}{i\omega_n - b_l} \end{aligned} \quad (16)$$

Using such a spectral representation our aim is to convert the usually complicated equations for $G(\mathbf{k}, i\omega_n)$ into sets of equations for the amplitudes $a_l^{\mathbf{k}}$ only.

A. Frequency grid

An important point is how to choose the frequency points b_l along the real axis. In a previous work [20] we let them fluctuate freely during the calculation but employed some approximations to restrict the number N_{max} . In this work we keep them fixed relative to the chemical potential which leads to an efficient algorithm. It also turned out to be of importance to adopt the frequency grid to the problem (e.g. if the influence of a band edge is important the frequency points should be more dense around that band edge) and especially to the temperature.

For a Fermionic system – where the energy range of $\pm k_B T$ around the chemical potential is of importance – we choose for the example discussed in section IV:

$$b_l = \frac{N_{max} - 1}{\beta \alpha} \tanh^{-1} \left(\frac{N_{max} - l}{N_{max} - 1} h_1 + \frac{l - 1}{N_{max} - 1} h_2 \right) \quad (17)$$

with

$$h_{1/2} = \tanh \left(\frac{\beta \alpha \omega_{min/max}}{N_{max} - 1} \right) \quad (18)$$

and ω_{min} and ω_{max} are the minimum and maximum frequencies considered, respectively. The parameter α was adjusted in the way that the distance between two frequency points around the chemical potential is always smaller than $k_B T$. In this way the delta functions are arranged with highest density at the chemical potential and far away from the chemical potential they get thinned out. Note that the index l does not need to have integer values – this will be used later on.

B. Products of correlation functions

Usually in such calculations we have to deal with products of correlation functions which can be folded both in momentum and frequency space. The result of such products of one-particle correlation functions are generalized susceptibilities. If we have two functions $G^1(\mathbf{k}, i\omega_n)$, $G^2(\mathbf{k}, i\omega_n)$, we often need to calculate the following product:

$$\begin{aligned} \chi(\mathbf{K}, i\Omega_m) &= -\frac{1}{\beta} \sum_n \frac{1}{N} \sum_{\mathbf{q}} \\ &G^1(\mathbf{q}, i\omega_n) G^2(\mathbf{K} - \mathbf{q}, i\Omega_m - i\omega_n) \end{aligned} \quad (19)$$

where \mathbf{K} is the total momentum of a pair of particles. We denote in the following Bosonic Matsubara frequencies and q-vectors of Bosons with upper-case letters whereas for Fermionic systems we use lower-case letters. $G^i(\mathbf{k}, i\omega_n)$, for $i = 1, 2$, has the approximate spectral representation:

$$G^i(\mathbf{q}, i\omega_n) \approx \sum_{j=1}^{N_{max}} \frac{a_j^{i, \mathbf{k}}}{i\omega_n - b_j} \quad (20)$$

We can directly evaluate the frequency summations and are left with sums over the coefficients. When inserting the spectral representation for $G^i(\mathbf{k}, i\omega_n)$ we get:

$$\begin{aligned} \chi(\mathbf{K}, i\Omega_n) &= -\sum_{\mathbf{q}} \sum_{j,l} \frac{1}{\beta} \sum_m \frac{a_l^{1, \mathbf{q}}}{i\Omega_n - i\omega_m - b_l} \frac{a_j^{2, \mathbf{K}-\mathbf{q}}}{i\omega_m - b_j} \\ &= \sum_{\mathbf{q}} \sum_{j,l} \frac{a_l^{1, \mathbf{q}} a_j^{2, \mathbf{K}-\mathbf{q}}}{i\Omega_n - b_j - b_l} \left(\frac{1}{1 + e^{\beta b_j}} - \frac{1}{1 + e^{-\beta b_l}} \right) \\ &= \frac{1}{2} \sum_{\mathbf{q}} \sum_{j,l} \frac{a_l^{1, \mathbf{q}} a_j^{2, \mathbf{K}-\mathbf{q}}}{i\Omega_n - b_j - b_l} \\ &\quad \left(\tanh \left(\frac{\beta b_j}{2} \right) + \tanh \left(\frac{\beta b_l}{2} \right) \right) \end{aligned} \quad (21)$$

We now have determined a spectral representation of $\chi(\mathbf{K}, Z)$ which is valid in the whole complex plane. Nonetheless, for convenience we continue writing our function on the Matsubara frequencies. $\chi(\mathbf{K}, i\Omega_n)$ is however defined via a spectral representation on $N_{max}(N_{max} + 1)/2$ frequency points along the real frequency axis which have to be folded back onto the N_{max} points of our frequency grid. Therefore we sort the $N_{max}(N_{max} + 1)/2$ points

$$\tilde{b}_{jl}^{\mathbf{K}} = b_j + b_l \quad , \quad (22)$$

check if they fit into each interval $b_{p-1/2} < \tilde{b}_{jl}^{\mathbf{K}} < b_{p+1/2}$ (the index of b in eq. (17) can be non integer) and add their amplitudes

$$\tilde{c}_{jl}^{\mathbf{K}} = a_l^{1, \mathbf{q}} a_j^{2, \mathbf{K}-\mathbf{q}} \left(\tanh \left(\frac{\beta b_j}{2} \right) + \tanh \left(\frac{\beta b_l}{2} \right) \right) \quad (23)$$

to the amplitude $c_p^{\mathbf{K}}$ of the susceptibility. In this way we obtain a similar spectral representation for the susceptibility:

$$\chi(\mathbf{K}, i\Omega_n) = \sum_{p=1}^{N_{max}} \frac{c_p^{\mathbf{K}}}{i\Omega_n - b_p} . \quad (24)$$

For the further calculation we just have to store the amplitudes $c_p^{\mathbf{K}}$. Note that if the $G^i(\mathbf{q}, i\omega_n)$, $i = 1, 2$ had been Fermionic correlation functions, the amplitudes $c_p^{\mathbf{K}}$ are – as opposed to the amplitudes $a_j^{i\mathbf{k}}$ – not only positive but change sign at the chemical potential due to the tanh function. The function $\chi(\mathbf{K}, i\Omega_m)$ will therefore be a Bosonic correlation function and $i\Omega_m$ are Bosonic Matsubara frequencies.

C. Vertex functions

Vertex functions $\Gamma(\mathbf{k}_1, \mathbf{k}_2, \dots, i\omega_{n1}, i\omega_{n2}, \dots)$ result from Bethe-Salpeter type equations and they are in general functionals of two particle propagators similar to the one described in subsection III B, of a correlation U_{corr} (which in general is a function of \mathbf{k} and ω as well) and of one particle correlation functions.

$$\Gamma(\mathbf{k}_1, \mathbf{k}_2, i\omega_{n1}, i\omega_{n2}) = \Gamma\{\chi(\mathbf{k}_1 + \mathbf{k}_2, i\omega_{n1} + i\omega_{n2}), \dots, U_{corr}, G(\mathbf{k}_i, i\omega_{ni}), \dots\} . \quad (25)$$

If they can be reduced to analytic functions in the complex plane they can be calculated by shifting the poles of the spectral representation at b_n into the upper half plane by an amount

$$\delta_n = \frac{1}{2}(b_{n+1/2} - b_{n-1/2}), \quad (26)$$

where the shift into the upper half plane depends on n and is smallest close to the chemical potential. With the help of such a vertex function a proper self-energy can be calculated in a way similar to the calculation of the susceptibility in subsection III B. In subsection IV A this is shown on the example of the attractive Hubbard model in the ladder approximation.

IV. EXAMPLE: ATTRACTIVE HUBBARD MODEL IN THE LADDER APPROXIMATION

The attractive Hubbard model shows superconductivity in its weak coupling 3D limit. The range of intermediate coupling and 2-3 dimensions is of particular interest for the high- T_c cuprates [12]. The Hubbard Hamiltonian is

$$H = -t \sum_{\langle i,j \rangle, \sigma} c_{i\sigma}^\dagger c_{j\sigma} + U \sum_i n_{i\uparrow} n_{i\downarrow}, \quad (27)$$

where t is the transfer integral between two neighbouring lattice sites $\langle i, j \rangle$ (we restrict ourselves to hyper-cubic lattices) and $U < 0$ is the attractive interaction for two electrons on the same site of the lattice. In the case of $U = 0$ the Hamiltonian can be diagonalized and gives the usual dispersion of a tight binding Hamiltonian $\epsilon(\mathbf{k})$. The non-interacting Green function $G^{(0)}(\mathbf{k}, i\omega_n)$ is approximated by the pole b_j which is nearest to $\epsilon(\mathbf{k})$.

$$G^{(0)}(\mathbf{k}, i\omega_n) \approx \frac{1}{i\omega_n - b_j} \quad (28)$$

$$b_{j-1/2} < \epsilon(\mathbf{k}) \leq b_{j+1/2} . \quad (29)$$

The ladder approximation [15] takes into account all non-crossing scattering events of a pair in the particle-particle channel and becomes exact for all coupling strengths in the low density limit $n \rightarrow 0$.

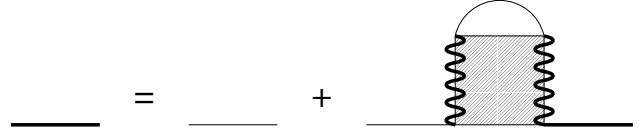


FIG. 1. schematic diagram of the non-self-consistent ladder equations. The full thick lines represent full, interacting Green functions, the thin lines non interacting Green functions and the wavy lines are the Hubbard interaction U .

This leads to the following system of equations [21] which has to be solved either non self-consistently (Eqs. (31)-(34)) which is diagrammatically shown in Fig. 1

$$G^{(0)}(\mathbf{k}, i\omega_n) = \frac{1}{i\omega_n - \epsilon(\mathbf{k})} \quad (30)$$

$$\chi^{(0)}(\mathbf{K}, i\Omega_m) = -\frac{1}{\beta} \sum_n \frac{1}{N} \sum_{\mathbf{q}} G^{(0)}(\mathbf{q}, i\omega_n) G^{(0)}(\mathbf{K} - \mathbf{q}, i\Omega_m - i\omega_n) \quad (31)$$

$$\tilde{\Gamma}^{(0)}(\mathbf{K}, i\Omega_n) = \frac{U^2 \chi^{(0)}(\mathbf{K}, i\Omega_n)}{1 - U \chi^{(0)}(\mathbf{K}, i\Omega_n)} + U \quad (32)$$

$$\Sigma^{(0)}(\mathbf{k}, i\omega_n) = \frac{1}{\beta} \sum_m \frac{1}{N} \sum_{\mathbf{q}} \tilde{\Gamma}^{(0)}(\mathbf{k} + \mathbf{q}, i\omega_n + i\omega_m) G^{(0)}(\mathbf{q}, i\omega_m) \quad (33)$$

$$G^{nsc}(\mathbf{k}, i\omega_n) = \frac{1}{G^{(0)}(\mathbf{k}, i\omega_n)^{-1} - \Sigma^{(0)}(\mathbf{k}, i\omega_n)} \quad (34)$$

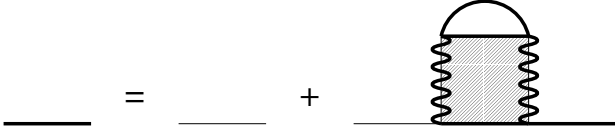


FIG. 2. schematic diagram of the fully self-consistent ladder equations.

or self-consistently (Eqs. (35)-(38)) which is diagrammatically shown in Fig. 2

$$\chi(\mathbf{K}, i\Omega_m) = -\frac{1}{\beta} \sum_n \frac{1}{N} \sum_{\mathbf{q}} G(\mathbf{q}, i\omega_n) G(\mathbf{K} - \mathbf{q}, i\Omega_m - i\omega_n) \quad (35)$$

$$\tilde{\Gamma}(\mathbf{K}, i\Omega_n) = \frac{U^2 \chi(\mathbf{K}, i\Omega_n)}{1 - U \chi(\mathbf{K}, i\Omega_n)} + U \quad (36)$$

$$\Sigma(\mathbf{k}, i\omega_n) = \frac{1}{\beta} \sum_m \frac{1}{N} \sum_{\mathbf{q}} \tilde{\Gamma}(\mathbf{k} + \mathbf{q}, i\omega_n + i\omega_m) G(\mathbf{q}, i\omega_m) \quad (37)$$

$$G(\mathbf{k}, i\omega_n) = \frac{1}{G^{(0)}(\mathbf{k}, i\omega_n)^{-1} - \Sigma(\mathbf{k}, i\omega_n)} \quad (38)$$

In order to obtain self-consistency the Eqs. (35)-(38) have to be calculated iteratively until a stable self-consistent solution is obtained.

A. Vertex function in the ladder approximation

In the case of the ladder approximation the vertex function (Eqs. (32),(36)) itself does not tend to zero as $\Omega \rightarrow \infty$, instead $\lim_{\Omega \rightarrow \infty} = U$. However the function $\tilde{\Gamma}(\mathbf{K}, i\Omega_m)$ can be decomposed into a function which fulfills Kramers-Kronig relations $\Gamma(\mathbf{K}, i\Omega_m)$ plus a constant U [22]. The function $\Gamma(\mathbf{K}, i\Omega_m)$ is U^2 times the two-particle propagator of a pair with total momentum \mathbf{K} . In order to obtain a spectral representation for $\Gamma(\mathbf{K}, z)$ we have two possibilities, which we now discuss in turn.

1. Complex evaluation

In the following we show the evaluation of $\Gamma(\mathbf{K}, z)$ in the complex plane. Therefore we need an approximate expression for the complex function $\chi(\mathbf{K}, z)$ at the frequency points b_m of our frequency grid of the real axis.

$$\chi(\mathbf{K}, b_m) \approx \sum_{n=1}^{N_{max}} \frac{c_m^{\mathbf{K}}}{b_m - b_n + i\delta_n} \quad (39)$$

with

$$\delta_n = \frac{1}{2}(b_{n+1/2} - b_{n-1/2}) \quad (40)$$

This has to be put into the equation for Γ

$$\Gamma(\mathbf{K}, b_m) \approx \frac{U^2 \chi(\mathbf{K}, b_m)}{1 - U \chi(\mathbf{K}, b_m)} \quad (41)$$

The amplitudes $g_m^{\mathbf{K}}$ of $\Gamma(\mathbf{K}, b_m)$ at the points b_m are then given by:

$$g_m^{\mathbf{K}} \approx \frac{2\delta_m}{\pi} \Im(\Gamma(\mathbf{K}, b_m)) \quad (42)$$

and we have obtained a spectral representation for $\Gamma(\mathbf{K}, b_m)$ which can be used for further calculation:

$$\Gamma(\mathbf{K}, i\Omega_m) \approx \sum_{n=1}^{N_{max}} \frac{g_m^{\mathbf{K}}}{i\Omega_m - b_n} \quad (43)$$

2. Evaluation with partial fractions

A second possibility to calculate the amplitudes $g_m^{\mathbf{K}}$ is by rewriting Eq. (41)

$$\Gamma(\mathbf{K}, \Omega) = \quad (44)$$

$$\frac{U^2 \sum_{n=1}^{N_{max}} \prod_{\substack{m=1 \\ m \neq n}}^{N_{max}} (\Omega - b_m) c_n^{\mathbf{K}}}{\prod_{n=1}^{N_{max}} (\Omega - b_n) - U \sum_{n=1}^{N_{max}} \prod_{\substack{m=1 \\ m \neq n}}^{N_{max}} (\Omega - b_m) c_n^{\mathbf{K}}} \quad (45)$$

and looking for the poles of the denominator. Since it is a polynomial of order N_{max} this seems to be a hopeless procedure. However the roots are bracketed between the old poles b_m and we know that the number of roots between $b_m^{\mathbf{K}}$ and $b_{m+1}^{\mathbf{K}}$ is one except at zero frequency where it can not exceed two. Therefore this problem can be solved numerically. Having found the roots $\tilde{b}_m^{\mathbf{K}}$ we can evaluate the amplitudes by putting the solution into the numerator of Eq. (44). This procedure is just calculating partial fractions for eq. (44). An analogous procedure as for the susceptibility (see Eq. (22)) allows us to calculate the amplitudes $g_m^{\mathbf{K}}$ at the frequency points b_m by adding all amplitudes for frequencies $\tilde{b}_m^{\mathbf{K}}$ in the interval $b_{m-1/2} < \tilde{b}_m^{\mathbf{K}} < b_{m+1/2}$.

Both methods IV A 1 and IV A 2 work well. In [20] we used method IV A 2 and for the calculations presented in this paper we use method IV A 1.

B. Self energy

Having calculated the vertex function $\Gamma(\mathbf{K}, i\Omega_m)$ we can proceed and calculate the self-energy $\Sigma'(\mathbf{k}, i\omega_n)$. The ' just reminds us that we do not calculate the full self-energy since we use $\Gamma(\mathbf{K}, i\Omega_m)$ instead of $\tilde{\Gamma}(\mathbf{K}, i\Omega_m)$. The inclusion of the frequency independent part (U) of the

vertex function will lead to the Hartree term. For the frequency dependent self-energy, we have

$$\begin{aligned}
\Sigma'(\mathbf{k}, i\omega_n) &= \\
& \frac{1}{N} \sum_{\mathbf{q}} \frac{1}{\beta} \sum_m \Gamma(\mathbf{k} + \mathbf{q}, i\omega_n + i\omega_m) G(\mathbf{q}, i\omega_m) \\
& \approx \frac{1}{N} \sum_{\mathbf{q}} \sum_{j,l}^{N_{max}} \frac{1}{\beta} \sum_m \frac{g_l^{\mathbf{k}+\mathbf{q}}}{i\omega_n + i\omega_m - b_l} \frac{a_j^{\mathbf{q}}}{i\omega_m - b_j} \\
& = \frac{1}{N} \sum_{\mathbf{q}} \sum_{j,l}^{N_{max}} \frac{g_l^{\mathbf{k}+\mathbf{q}} a_j^{\mathbf{q}}}{i\omega_n - b_l + b_j} \left(\frac{1}{1 + e^{\beta b_j}} + \frac{1}{e^{\beta b_j} - 1} \right) \quad (46)
\end{aligned}$$

The Bosonic distribution function is due to the Bosonic nature of a pair of Fermions described by $\Gamma(\mathbf{K}, i\Omega_m)$. Again an analogous procedure as for the susceptibility (see Eq. (22)) yields the coefficients $s_j^{\mathbf{k}}$ at the frequencies b_j of our frequency grid. In this way we obtain a spectral representation for the self-energy

$$\Sigma'(\mathbf{k}, i\omega_n) = \sum_{n=1}^{N_{max}} \frac{s^{\mathbf{k}}}{i\omega_n - b_j} \quad (47)$$

C. Calculation of the full Green function

Knowing the self-energy $\Sigma(\mathbf{k}, i\omega_n)$ we can calculate the Green function for the one-particle propagator.

$$\begin{aligned}
G(\mathbf{k}, i\omega_n) &= (i\omega_n - \epsilon(\mathbf{k}) + \mu - \Sigma(\mathbf{k}, i\omega_n))^{-1} \\
& \approx \left(i\omega_n - \epsilon(\mathbf{k}) + \mu - \sum_{j=1}^{N_{max}} \frac{s^{\mathbf{k}}}{i\omega_n - b_j} \right)^{-1} \quad (48)
\end{aligned}$$

Again we have two alternatives to calculate a spectral representation for $G(\mathbf{k}, i\omega_n)$. Analogous to the case IV A 1 when calculating the vertex function from the susceptibility we get for the amplitudes of the one-particle Green function,

$$\begin{aligned}
a_m^{\mathbf{k}} &= \frac{2\delta_m}{\pi} \Im(G(\mathbf{k}, b_m)) \\
& \approx \frac{2\delta_m}{\pi} \Im \left(b_m - \epsilon(\mathbf{k}) + \mu - \sum_{j=1}^{N_{max}} \frac{s_n^{\mathbf{k}}}{b_m - b_j + i\delta_j} \right)^{-1} \quad (49)
\end{aligned}$$

where δ_n is defined in Eq. (40). Due to the approximations made the sum rules might not always be fulfilled. Therefore it is necessary to perform a sum rule check and correct (if needed) the amplitudes $a_m^{\mathbf{k}}$.

D. Self-consistent vs. non-self-consistent

Going once through the procedure Eqs. (31)-(34) we obtain a non-self-consistent result which is conserving in

a one-particle picture (the equation $0 < N < 2$ with N the total particle number is fulfilled for all possible values of μ and T). Already this is an improvement to the solution of the T-matrix equations given by Schmitt-Rink et al. [23], as advocated by Serene [24].

It is also possible to go iteratively through the Eqs. (35)-(38). In this case the amplitudes will need an additional index p for the number of iterations.

$$a_j^{\mathbf{k}} \longrightarrow a_j^{\mathbf{k},p} \quad , \quad c_j^{\mathbf{K}} \longrightarrow c_j^{\mathbf{K},p} \quad , \quad \dots \quad (50)$$

Now the Eqs. (35)-(38) just map the amplitudes to the next level of iteration.

$$a_j^{\mathbf{k},p} \longrightarrow a_j^{\mathbf{k},p+1} \quad , \quad c_j^{\mathbf{K},p} \longrightarrow c_j^{\mathbf{K},p+1} \quad , \quad \dots \quad (51)$$

This procedure has to be repeated until a stable self-consistent solution is achieved. As a condition for self-consistency we used:

$$\frac{1}{N_{max}} \frac{1}{N_{\mathbf{K}}} \left(\sum_{\mathbf{k}} \sum_{j=1}^{N_{max}} ((a_j^{\mathbf{k},p})^2 - (a_j^{\mathbf{k},p+1})^2) \right)^{1/2} < \delta \quad (52)$$

were δ was typically chosen around 10^{-7} .

V. NUMERICAL DISCUSSION OF SPECTRAL QUANTITIES

In the following we will present several dynamical quantities which were obtained by using a numerical solution of the equations of the T-matrix in the ladder approximation for the attractive Hubbard model on a 2D square lattice.

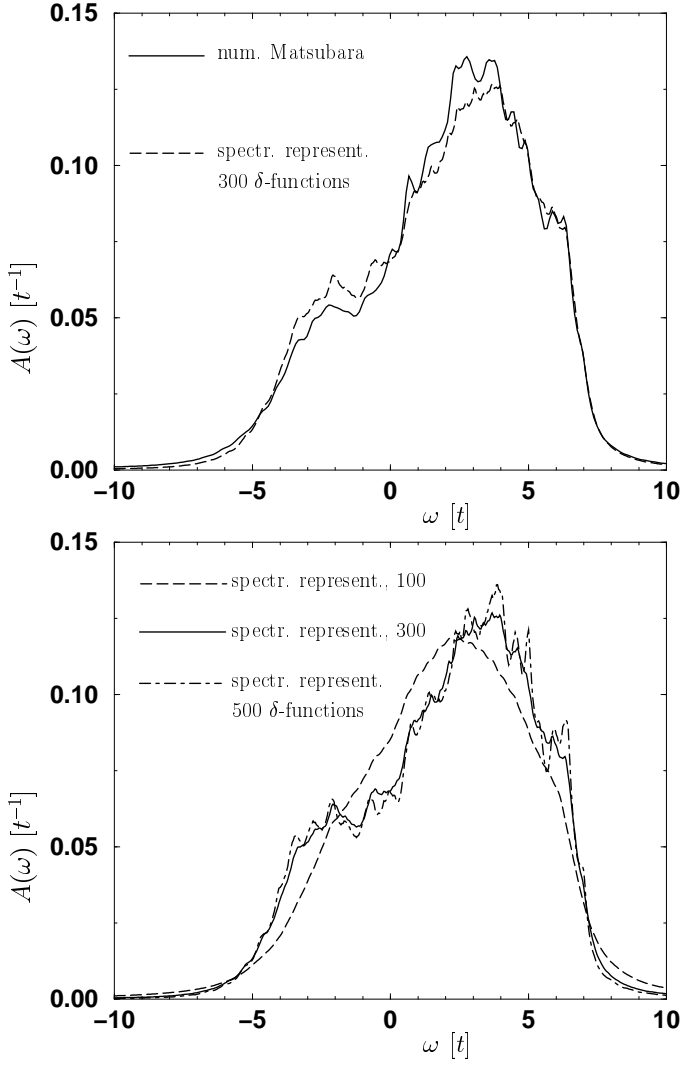


FIG. 3. For a 8×8 cubic 2D lattice, $k_B T = 0.55[t]$, $U = -4[t]$, $\mu = -2[t]$ and $n \approx 0.7$ the density of states is plotted. $\omega = 0$ is the position of the chemical potential. In (a) the full line corresponds to results obtained with Matsubara technique and Pade approximates and the dashed line is the result of our spectral representation technique for $N_{max} = 300$. In (b) we compare different numbers of $N_{max} = 100, 300, 500$.

In Figs. 3 and 4 we compare the density of states for a non-self-consistent calculation (Eqs. (31)–(34)) on an 8×8 lattice. The temperature was chosen to $0.55[t]$ and the attractive interaction $U = -4[t]$ which is half the bandwidth of the non-interacting system. The chemical potential was fixed to $\mu = -2[t]$ which led to an electron density of $n \approx 0.7$ at this temperature.

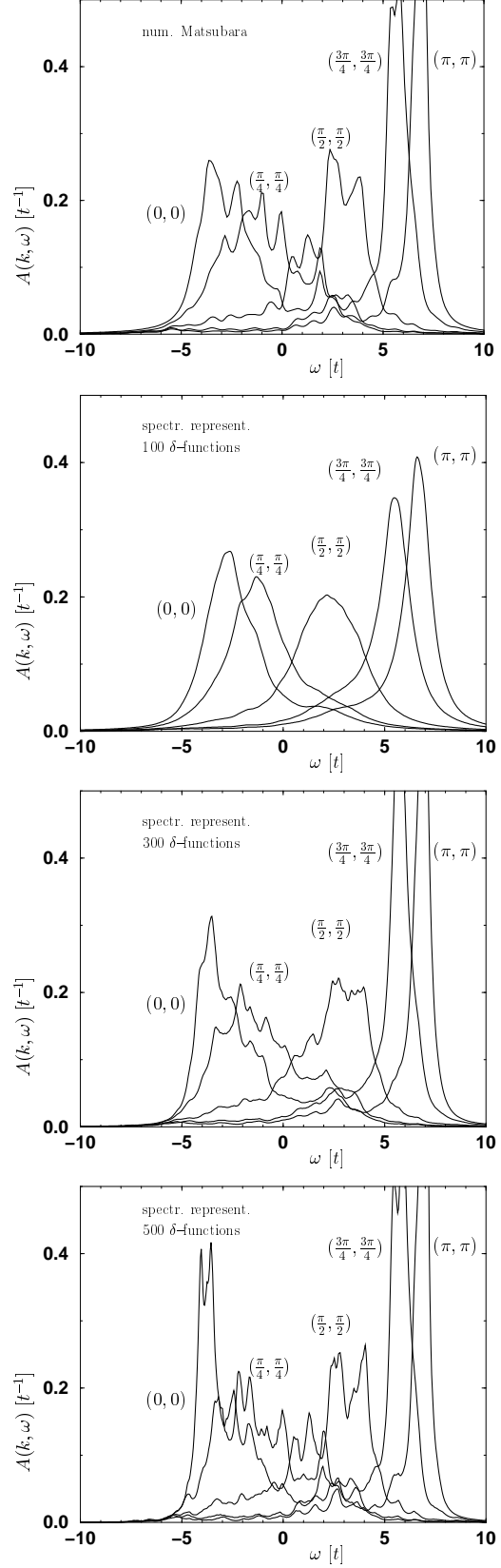


FIG. 4. For the same parameters as in Fig. 3 the \mathbf{k} dependent spectral function along the (1, 1) direction is plotted. (a) shows the result from the Matsubara technique whereas (b-d) contain the result for $N_{max} = 100, 300, 500$ respectively.

For the spectral representation technique we used a frequency range of (see Eq. (18)) $\omega_{min} = -24[t] < \omega < \omega_{max} = 24[t]$, the parameter α in Eq. (18) was chosen to be $\alpha = 2$ and we discuss the effect of a different number of δ -functions N_{max} . In Fig. 3a we compare the density of states as obtained with Matsubara technique and a numerically exact analytic continuation onto the real axis [17] which is possible only for the non-self-consistent calculation with a calculation for $N_{max} = 300$. At $\omega - \mu = 2[t]$ there is a remnant of the logarithmic singularity which occurs in the middle of the band of a non-interacting 2D system. Below that, around $\omega = 0$ and below the chemical potential clear correlation effects can be seen which lead to additional states at $\omega < 0$. In Fig. 3b we compare for the same parameters different numbers N_{max} of δ -peaks. For $N_{max} = 100$ the correlation effects around the chemical potential are not clearly visible whereas for $N_{max} = 300$ they are clearly present. Increasing N_{max} up to 500 does not alter the picture.

In Fig. 4 we calculate \mathbf{k} dependent quantities along the (1, 1) direction. The results from the Matsubara technique show that there is a strong incoherent broadening of the former quasiparticle peak around k_F and for $k < k_F$ due to correlations. Along the diagonal the Fermi wave-vector is bracketed by $(\pi/4, \pi/4) < k_F < (\pi/2, \pi/2)$. Already the calculation with $N_{max} = 100$ in Fig. 4b resolves the incoherent broadening but does fail to give further details which are clearly visible in the calculation for Fig. 4c for $N_{max} = 300$ and in Fig. 4d for $N_{max} = 500$.

In order to demonstrate the strength of our method we discuss in the following (Figs. 5 - 12) some aspects of the temperature dependence of the correlation functions obtained for a 16x16 lattice with $N_{max} = 300$, $\omega_{min} = -32[t]$ and $\omega_{max} = 32[t]$ (see Eq. (18)). The strength of the attractive interaction for these figures is $U = -8[t]$, which is equal to the bandwidth of the non-interacting system. The particle number was chosen to be $n = 0.2$ ($n = 1$ would correspond to half filling) and the chemical potential was adjusted as a function of temperature in order to keep the particle number n constant. In Figs. 5-8 non-self-consistent results according to Eqs. (31)-(34) are presented whereas in Figs. 9-12, results from a fully self-consistent calculation are presented.

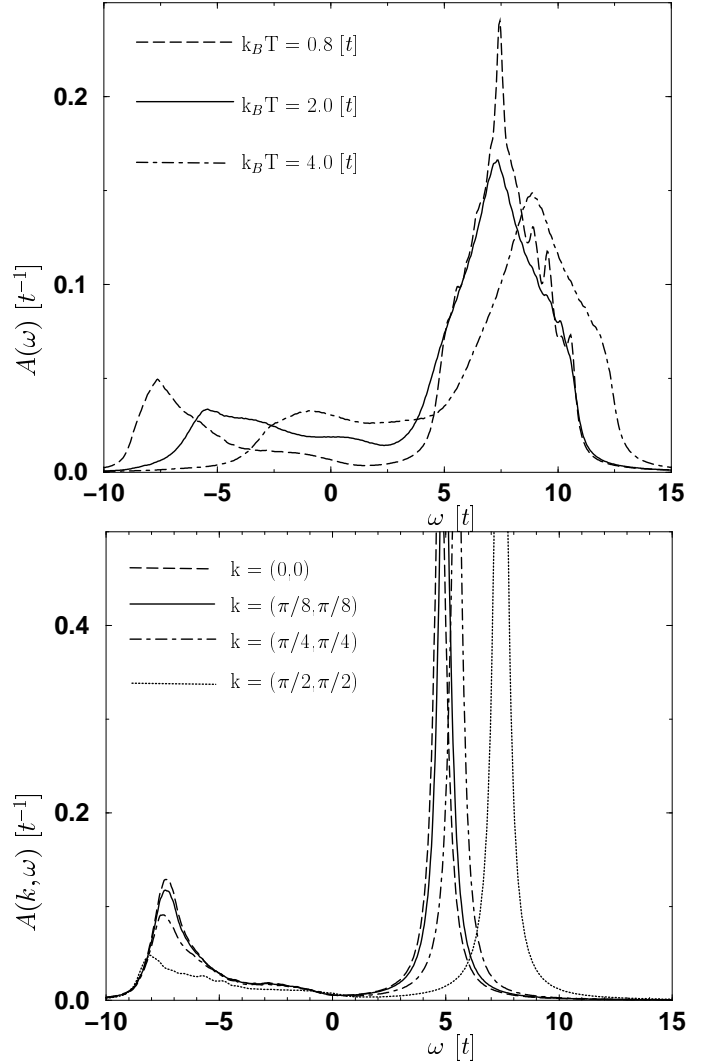


FIG. 5. For a 16x16 cubic 2D lattice, $U = -8[t]$ and $n = 0.2$ the density of states is plotted for three different temperatures. the chemical potential μ has been adjusted as a function of temperature to keep n constant. $\omega = 0$ is the position of the chemical potential. (a) shows the density of states for the three temperatures $k_B T = 4.0[t]$ (dot-dashed line), $k_B T = 2.0[t]$ (full line) and $k_B T = 0.8[t]$ (dashed line). (b) shows for the lowest temperature the \mathbf{k} -dependent spectral function along the (1, 1) direction. The results were obtained with a non-self-consistent calculation.

Fig. 5a shows the \mathbf{k} -integrated density of states. With decreasing temperature a gap occurs. The density at higher temperatures results from the one-particle continuum and the density for low energies results from pairs in a two-particle bound state. Fig. 5b shows that for $k_B T = 0.8[t]$ also the \mathbf{k} -dependent spectral function consists of two parts especially around $k = k_F$,

$$k_F \approx (\pi/8, \pi/8).$$

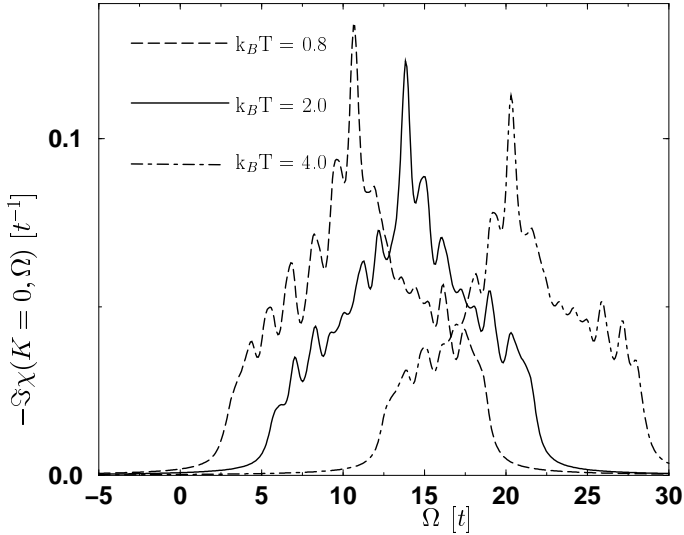


FIG. 6. For the same parameters as in Fig. 5 the imaginary part of the susceptibility for pairs of electrons with total momentum $K = 0$ is shown as obtained from a non-self-consistent calculation.

Fig. 6 shows the imaginary part of the susceptibility for a total momentum of the pair of $K = 0$ which is – as it should be – the non-interacting density of states where the energy has been stretched by a factor of 2. It is simply shifted according to the shift of the chemical potential with temperature. Due to the low density in the example we have chosen the chemical potential does not enter in the one-particle continuum. This is the case for higher densities where the imaginary part of the susceptibility changes sign at zero.

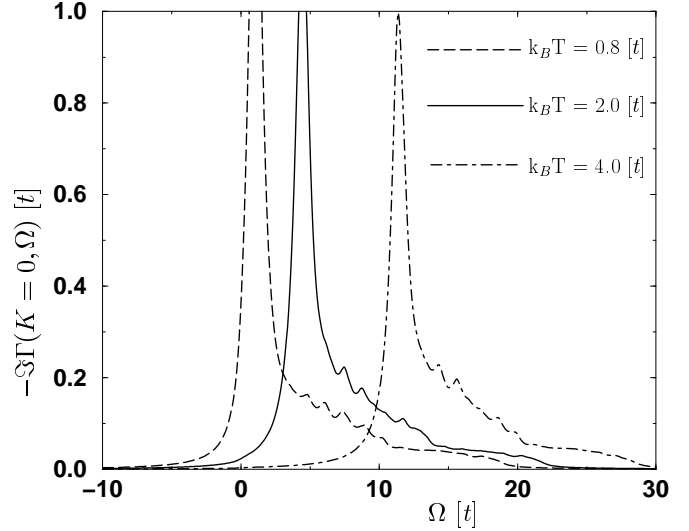


FIG. 7. For the same parameters as in Fig. 5 the imaginary part of the vertex function $\Gamma(\mathbf{K} = \mathbf{0}, \Omega)$ for pairs of electrons with total momentum $K = 0$ is shown as it results from a non-self-consistent calculation.

Fig. 7 shows the imaginary part of the vertex function $\Gamma(K = 0, \Omega)$. The strong peak corresponds to a true bound state and with decreasing temperature, the chemical potential drifts towards the bound state indicating Bose condensation of non-interacting pairs into the bound state.

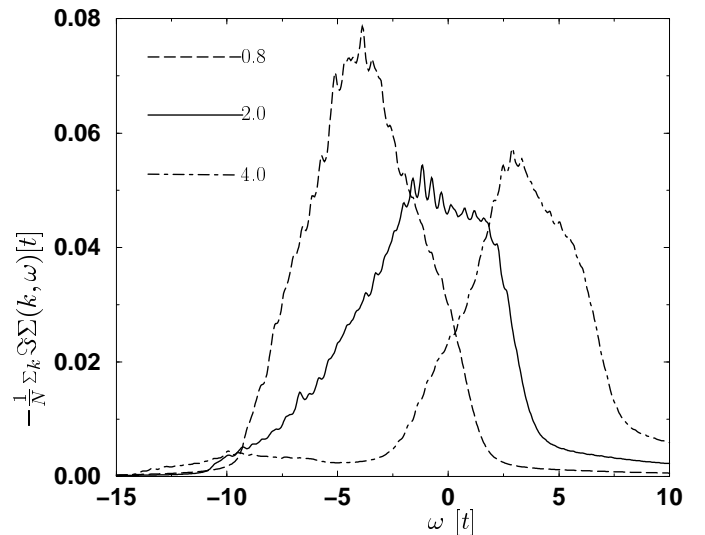


FIG. 8. For the same parameters as in Fig. 5 the imaginary part of the \mathbf{k} -averaged self-energy is shown as it results from a non-self-consistent calculation.

In Fig. 8 we show the k -averaged imaginary part of the self-energy $\Sigma(k, \omega)$. It mainly shifts with the chemical potential but does not otherwise show a large temperature dependence.

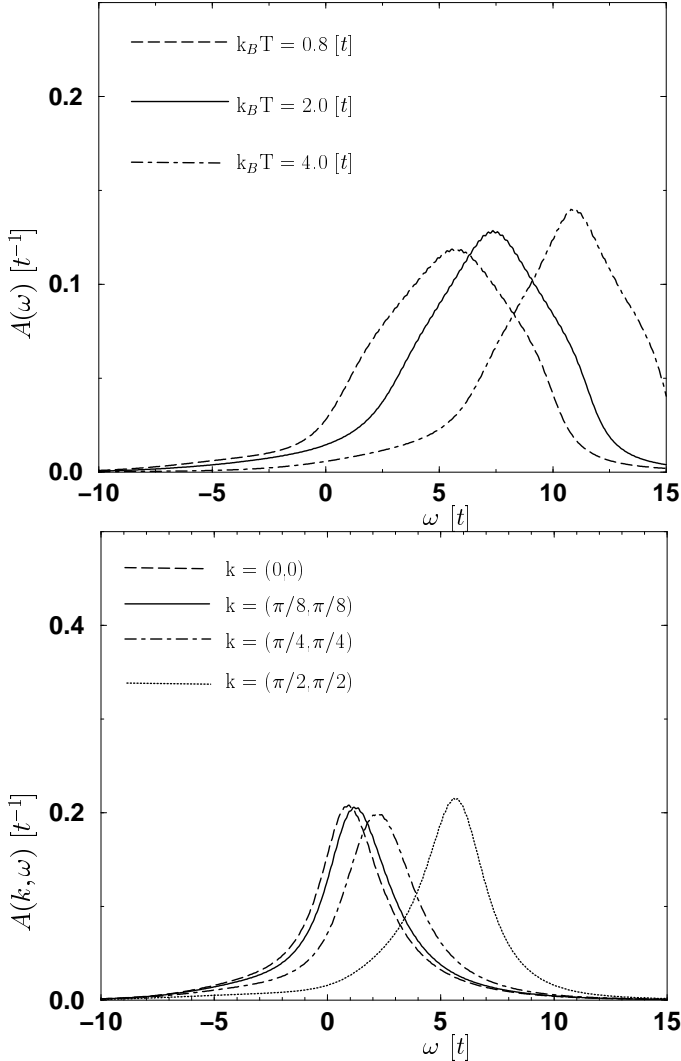


FIG. 9. For the same parameters as in Fig. 5 the density of states resulting from a fully self-consistent calculation is plotted in (a), while (b) shows the \mathbf{k} -dependent spectral function.

In the following figures we show results from a self-consistent calculation which have to be compared with the results from the non-self-consistent calculation. Fig. 9a shows the density of states. Even though it looks similar for $k_B T = 4[t]$ there is strong difference at lower temperatures. The gap is no longer present due to the self-consistent procedure. Also for the \mathbf{k} -dependent spectral functions (for $k_B T = 0.8[t]$ in Fig. 9b) there is no

splitting into two parts.

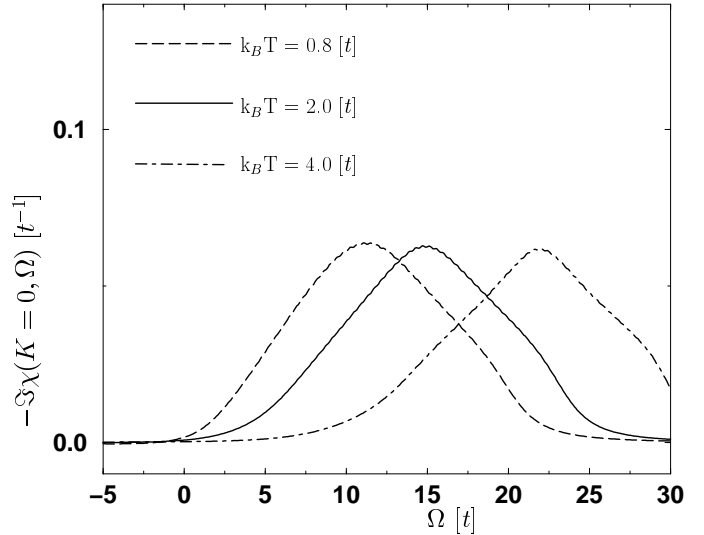


FIG. 10. For the same parameters as in Fig. 5 the imaginary part of the susceptibility for pairs of electrons with total momentum $K = 0$ is shown as it results from a fully self-consistent calculation.

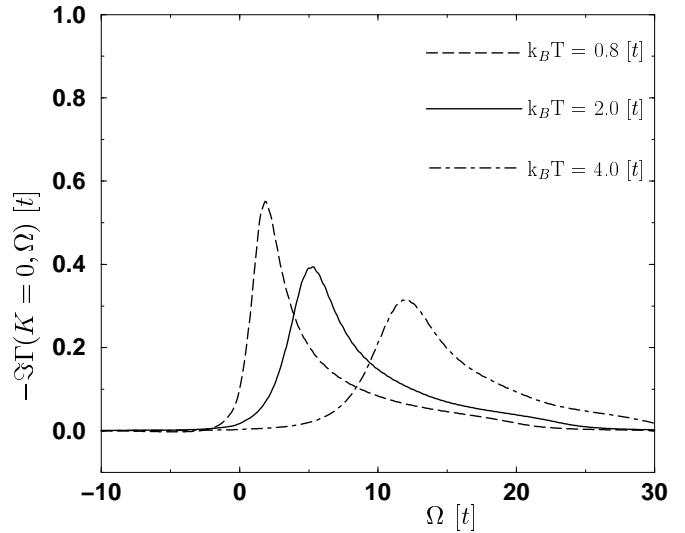


FIG. 11. For the same parameters as in Fig. 5 the imaginary part of the vertex function $\Gamma(\mathbf{K} = \mathbf{0}, \Omega)$ for pairs of electrons with total momentum $K = 0$ is shown as it results from a fully self-consistent calculation.

Fig. 10 shows the imaginary part of the susceptibility. It is no longer an image of the non-interacting density of states. Note that it becomes negative for $\Omega < 0$ at

the lowest temperature considered here ($k_B T = 0.8[t]$) which is barely visible from the plot and indicates that the chemical potential is now in the one particle continuum. Also the imaginary part of the vertex function $\Gamma(\mathbf{K}, \Omega)$, which is plotted for $\mathbf{K} = 0$ in Fig. 11, changes sign at $\Omega = 0$, although this seems to happen in the plot (Fig. 11) for $\Omega < 0$, which is just an artifact of the broadening of the δ -functions which had to be applied in order to plot a spectral quantity. The peak in $\Im\Gamma(\mathbf{K} = 0, \Omega)$ no longer corresponds to a bound state; it is a two particle resonance in the one-particle continuum.

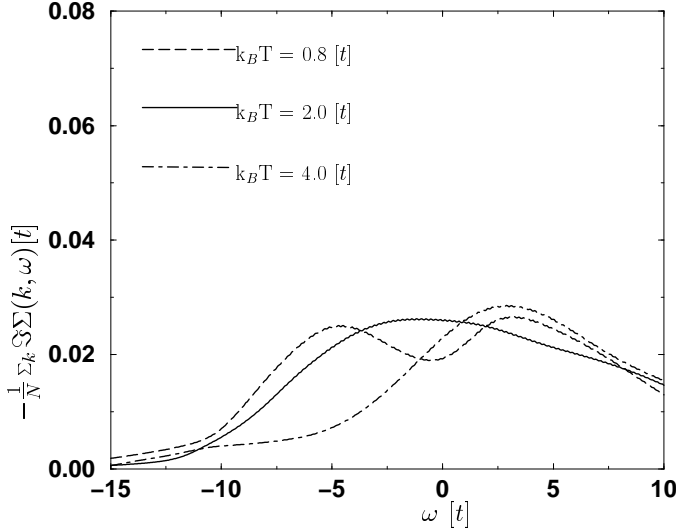


FIG. 12. For the same parameters as in Fig. 5 the imaginary part of the \mathbf{k} -averaged self-energy is shown as it results from a fully self-consistent calculation.

Also the self-energy whose imaginary part is (averaged over \mathbf{k}) plotted in Fig. 12 is strongly altered due to self-consistency. Compared to the non-self-consistent part in Fig. 8 it is strongly decreased in magnitude and starts at low temperatures to develop a minimum at $\omega = 0$ indicating the appearance of Fermi liquid like properties.

VI. CONCLUSION

Using the example of the attractive Hubbard model we have evaluated the ladder diagrams of the T-matrix, and we have demonstrated that our numerical method, which works entirely along the real frequency axis, enables us to accurately calculate spectral properties. We should point out that we did not show results for the lowest temperatures we were able to reach. In fact we can decrease the temperature for the calculations of Figs. 5 - 12 by an additional two orders of magnitude without reaching numerical instabilities. However these results and especially their physical interpretation are not the main subject of

the current paper. Here we have described in detail the numerical method and discussed its applicability to solve different problems of correlated quantum systems.

ACKNOWLEDGMENTS

We acknowledge financial support from the BMBF, Germany. M.L. further thanks R. J. Gooding for pointing out the importance of the T-matrix calculation and for stimulating discussions.

-
- [1] D. N. Zubarev. *Usp. Fiz. Nauk* (71)71 [Secs 25, 31], (1960).
 - [2] S. V. Tyablikov. *Methods in the Quantum theory of Magnets*. Plenum Press, New York, (1967).
 - [3] T. Matsubara. *Prog. Theor. Phys.* **14**, 351, (1955).
 - [4] J. R. Schrieffer, D. J. Scalapino and J. W. Wilkins. *Phys. Rev. Lett.* **10** 336, (1963).
 - [5] D. J. Scalapino, J. R. Schrieffer, and J. W. Wilkins. *Phys. Rev.* **148** 263, (1966).
 - [6] C. S. Owen and D. J. Scalapino. *Physica (Amsterdam)* **55** 691, (1971).
 - [7] G. Bergmann and D. Rainer. *Z. Physik* **263** 59, (1973).
 - [8] D. Rainer and G. Bergmann. *J. Low Temp. Phys.* **14** 501, (1974).
 - [9] J. W. Serene H. J. Vidberg. *J. of Low Temp. Phys.* **29**(3/4) 179, (1977).
 - [10] R. N. Silver, J. E. Gubernatis, D. S. Sivia, M. Jarrell. *Phys. Rev. Lett.* **65**, 496, (1990).
 - [11] M. Randeria et al. *Phys. Rev. Lett.* **62** 981, (1989).
 - [12] R. Micnas, M.H. Pedersen, S. Schafroth, T. Schneider, J.J. Rodriguez-Nunez, H. Beck. *Phys. Rev. B* **52** 16223, (1995).
 - [13] B. Janko, J. Maly, K. Levin. *Phys. Rev. B* **56** R11407, (1997).
 - [14] A cleaner mathematical definition allows to define the frequency dependent Green function as the complex Laplace transform of the thermal expectation value of the commutator between two operators $\langle [C(t-t'), B]_{\mp} \rangle$.
 - [15] J. D. Walecka A. L. Fetter. *Quantum Theory of Many-Particle Systems*. McGraw-Hill, (1971).
 - [16] I. E. Dzyaloshinski A. A. Abrikosov, L. P. Gorkov. *Methods of quantum field theory in statistical physics*. Dover, (1975).
 - [17] F. Marsiglio, M. Schossmann and J. P. Carbotte. *Phys. Rev. B* **37** 4965, (1988).
 - [18] R. Fresard, B. Glaser, P. Wölfle. *J. Phys. Cond. Mat.* **4** 8565, (1992).
 - [19] Bumsoo Kyung, E.G. Klepfish, P.E. Kornilovitch. *Phys. Rev. Lett.* **80**(14) 3109, (1998).
 - [20] M. Letz, R. J. Gooding. *J. Phys. Cond. Mat.* **10** (31) 6931-6951, (1998).
 - [21] R. Haussmann. *Z. Phys. B* **91** 291, (1993).

- [22] D. J. Thouless. *Annals of Phys.* **10** 553, (1960).
- [23] S. Schmitt-Rink, C. M. Varma, A. E. Ruckenstein.
Phys. Rev. Lett. **63**, 445, (1989).
- [24] J. W. Serene. *Phys. Rev. B* **40**(16) 10873, (1989).